Engineering Analysis with Boundary Elements 84 (2017) 220–230

Contents lists available at ScienceDirect

Engineering Analysis with Boundary Elements

journal homepage: www.elsevier.com/locate/enganabound

Transient SH-wave scattering by the lined tunnels embedded in an elastic half-plane

Mehdi Panji*, Bahman Ansari

Department of Civil Engineering, Zanjan Branch , Islamic Azad University, Zanjan, Iran

ARTICLE INFO

Keywords:
Half-plane BEM
Time-domain
Single/twin lined tunnels
SH-wave
Seismic analysis
Surface response

ABSTRACT

A direct half-plane time-domain boundary element method (BEM) was developed and successfully applied to analyze the transient response of ground surface in the presence of arbitrarily shaped lined tunnels, embedded in a linear elastic half-space, subjected to propagating obliquely incident plane SH-waves. To prepare the model, only the interface and inner boundary of the lining need to be discretized. The problem was decomposed into a pitted half-plane and a closed ring-shaped domain, corresponding to the substructure procedure. After computing the matrices and satisfying the compatibility as well as boundary conditions, the coupled equations were solved to obtain the boundary values. To validate the responses, a practical example was analyzed and compared with those of the published works. The results showed that the model was very simple and the accuracy was favorable. Advanced numerical results were also illustrated for single/twin circular lined tunnels as synthetic seismograms and three-dimensional frequency-domain responses. The method used in this paper is recommended to obtain the transient response of underground structures in combination with other numerical methods.

1. Introduction

According to the extensive development of urban texture and the vital necessity of lifelines, infrastructure and underground openings have found an important role in human societies. A full understanding of the behaviors of underground tunnels including tunnels for transportation, water, and facilities, can assist in presenting an optimum layout. The importance of this issue has increased because of the complex performance of the tunnels against seismic loads. The seismic analysis of underground tunnels has been used by the researchers for almost half a century. A complete review up to 1981 can be found in Ariman and Muleski [1] about the methods employed for analyzing the ground with underground tunnels. Apart from experimental and field approaches, solution methods can be divided into three categories: analytical, semi-analytical, and numerical [2].

To analyze the ground response in the presence of unlined and lined tunnel cases, analytical and semi-analytical methods were developed as well. Lee [3], Datta and Shah [4], Lee et al. [5], Tsuar and Chang [6], and Gao et al. [7] investigated the unlined tunnels subjected to seismic waves by analytical approaches. The seismic analysis of a single-phase medium including a lined tunnel was presented in the analytical studies of Lee and Trifunac [8], Balendra et al. [9], Smerzini et al. [10], Zhang et al. [11], Li et al. [12], Min and Bing-Yu [13], Liu et al. [14], Xu et al. [15], and Yi et al. [16]. In the use of analytical procedures, the problem of lined tunnel embedded in a multi-phase medium was explored by Shi et al. [17], Hasheminejad and Kazemirad [18], and Jiang et al. [19]. In this regard, some studies can be found in the literature on modeling the embedded lined tunnels with the help of semi-analytical approaches which include Datta et al. [20], Wong et al. [21], Chin et al. [22], Moore and Guan [23], Manoogian [24], Davis et al. [25], Yeh et al. [26], Liao et al. [27], and Liu et al. [28] in a single-phase medium, and Zhou et al. [29] in a multi-phase medium.

According to what is observed in the nature, although the responses of analytical or semi-analytical methods have a high accuracy, various types of arbitrarily shaped topographic features cannot be applied for modeling in reality. It results in the development of numerical methods with a good flexibility. Generally, these methods can be divided into two types of volumetric and boundary methods. Despite the development of volumetric methods such as finite element method (FEM) or finite difference method (FDM) and their simple formulations, the whole body including the inside and boundaries must be discretized in order to model unlined/lined underground tunnels and topographies (e.g. Besharat et al. [30]; Esmaeili et al. [31]; Faccioli et al. [32]; Gelagoti et al. [33]; Huang et al. [34]; Narayan et al. [35]; Rabeti and Baziar [36]; Yiouta-Mitra et al. [37]). As a result, special attention has been paid to the boundary element method (BEM) among the various existing numerical methods in the recent three decades. Full reviews of BEM and its application can be respectively found in Beskos [38] and Stamos and Beskos [39] for underground structures.

* Corresponding author.
E-mail addresses: m.panji@iauz.ac.ir (M. Panji), bahman.ans@chmail.com (B. Ansari).

http://dx.doi.org/10.1016/j.enganabound.2017.09.002
Received 18 March 2017; Received in revised form 4 September 2017; Accepted 5 September 2017
0955-7997/

In order to model underground tunnels using BEM approaches, the surrounding boundaries must be discretized. If the two-dimensional BEM formulation was established based on a full-plane scenario, the circumference of the unlined/lined tunnel, smooth ground surface, and enclosing boundary must be meshed [40]. In this regard, full-plane BEM was statically used by Crouch and Starfield [41], Yang and Sterling [42], Xiao and Carter [43], Panji et al. [44], Wu et al. [45], and Panji et al. [46] for modeling underground tunnels. Also, this method was dynamically utilized to analyze the seismic behavior of the ground including unlined/lined tunnels in the transformed domains (e.g. Kattis et al. [47]; Liu and Liu [48]; Luco and de barros [49]; Manolis and Beskos [50]; Parvanova et al. [51]; Yu and Dravinski [52]).

When the stress-free boundary conditions on the smooth ground surface are satisfied and applied in the formulation, the half-plane BEM scenario is obtained [53]. Although the formulation became more complex, the accuracy and modeling were improved. In the use of this method, only the boundaries around the unlined/lined tunnel need to be discretized. Similar to the full-plane case, half-plane BEM was developed in both static and dynamic states. Some researchers statically utilized this method to analyze half-plane problems in the presence of underground tunnels as well as inhomogeneities (e.g. Dong et al. [54]; Dong and Lo [55]; Panji and Ansari [56]; Telles and Brebbia [57]; Ye and Sawada [58]). In the frequency domain, half-plane BEM was dynamically applied to obtain the seismic ground response with unlined/lined tunnels (Ba and Yin [59]; Benites et al. [60]). Despite the fact that the formulation of the method in the time-domain is more difficult, analyzing the problems with time-dependent geometry and the ability to combine with other numerical approaches can be only achieved in the use of transient responses. Most studies carried out using time-domain BEM were not only formulated in the full-plane, but also applied to investigate surface topographies and unlined tunnels (e.g. Alielahi et al. [61]; Kamalian et al. [62–64]; Takemia and Fujiwara [65]). To the best knowledge of the present authors, in the few studies using half-plane time-domain BEM, the lined tunnel problem embedded in a half-plane has not been studied so far (Belytschko and Chang [66]; Hirai [67]; Panji et al. [53,68,69]; Rice and Sadd [70]).

This paper develops a half-plane time-domain BEM for analyzing seismic ground response in the presence of arbitrarily shaped underground lined tunnels subjected to propagating obliquely incident SH-waves. By the assistance of an appropriate substructuring process, the model was decomposed into a half-plane with a cavity and a closed ring-shaped medium. After applying the method for each domain and obtaining the influence coefficients of the matrices, continuity and boundary conditions were used to determine the assembled coupled equation. The method was successfully implemented in a developed algorithm previously called as DASBEM [53]. The capability and efficiency of the method as well as the prepared computer code were investigated by solving a practical example and comparing the results with those of the published works. With considering some intended parameters, a numerical study was eventually conducted to obtain the ground surface response including single/twin circular lined tunnels. Displaying a powerful approach for preparing simple models of underground lined tunnels, determining accurate results in the use of the proposed method, and presenting some applicable graphs to complete the results were the main purposes of the present paper.

2. Statement of the problem

Consider a homogeneous linear elastic half-plane including an arbitrarily shaped underground lined tunnel as shown in Fig. 1. It is assumed that the lining and surrounding domain have a perfect interaction. The governing scalar wave equation and existing boundary conditions on the smooth ground surface are respectively as follows [71]:

$$\frac{\partial^2 u(x,y,t)}{\partial x^2}+\frac{\partial^2 u(x,y,t)}{\partial y^2}+b(x,y,t)=\frac{1}{c^2}\frac{\partial^2 u(x,y,t)}{\partial t^2} \tag{1}$$

and:

$$\mu\frac{\partial u(x,y,t)}{\partial n}\Big|_{y=0}=0 \tag{2}$$

where $u(x, y, t)$ and $b(x, y, t)$ are antiplane displacement and body force at point (x, y) and current time t, respectively; c is shear wave velocity given by $\sqrt{\mu/\rho}$, with μ as shear modulus and ρ as mass density; and n is the normal vector for the ground surface. As can be seen in Fig. 1, the model is decomposed into two domains, a uniform half-plane with arbitrarily shaped unlined cavity, and a closed ring-shaped medium. To solve the problem, half-plane time-domain BEM must be applied for each domain, using the image source approach to define a complementary area. Moreover, Fig. 1 depicts the meshing form using the proposed method located only on the surrounding boundaries.

3. Half-plane time-domain BEM

The key parameters of BEM approaches are the solutions obtained from basic equations. Transient half-plane fundamental solutions can be achieved by the singular solution of Eq. (1) and considering Eq. (2). These solutions can be found in Panji et al. [53]. If the problem is statically solved, fundamental solutions are adequate for the formulating process. An application of elastostatic half-plane BEM in modeling lined tunnels can be found in Panji and Ansari [56].

3.1. Boundary integral equation (BIE)

The original form of the direct time-domain boundary integral equation (BIE) can be obtained by applying the weighted residual integral to Eq. (1) and ignoring the contributions from initial conditions and body forces [72,73]. If the problems include incoming waves, the original BIE must be modified [74,75]. The modified form of BIE is as follows:

$$c(\boldsymbol{\xi})u(\boldsymbol{\xi},t)=\int_\Gamma\left\{\int_0^t\left[u^*(\boldsymbol{x},t;\boldsymbol{\xi},\tau).q(\boldsymbol{x},\tau)-q^*(\boldsymbol{x},t;\boldsymbol{\xi},\tau).u(\boldsymbol{x},\tau)\right]d\tau\right\}\times d\Gamma(\boldsymbol{x})+u^{ff}(\boldsymbol{\xi},t) \tag{3}$$

u^* and q^* are half-plane time-domain displacement and traction fundamental solutions at position $\boldsymbol{x}$ and time t due to a unit antiplane impulsive force in position $\boldsymbol{\xi}$ and preceding time τ, respectively [53]; u and q are displacements and tractions of boundary, respectively; $\Gamma(\boldsymbol{x})$ denotes the boundary of the body; $c(\boldsymbol{\xi})$ is the geometry coefficient; and u^{ff} is the free field displacement of ground surface without surface irregularities.

3.2. Discretizing BIE

To solve BIE and carrying out the integrations, the time axis and the boundary of the body must be discretized. By discretizing the time axis using N equal increments with duration Δt ($t=N\,\Delta t$), temporal integration can be analytically accomplished. With assuming a linear variation for the temporal shape functions, the following form of BIE can be obtained:

$$c(\boldsymbol{\xi})u^N(\boldsymbol{\xi})=\sum_{n=1}^{N}\int_\Gamma\begin{pmatrix}\left[U_1^{N-n+1}(\boldsymbol{x},\boldsymbol{\xi})+U_2^{N-n}(\boldsymbol{x},\boldsymbol{\xi})\right]q^n(\boldsymbol{x})\\-\left[Q_1^{N-n+1}(\boldsymbol{x},\boldsymbol{\xi})+Q_2^{N-n}(\boldsymbol{x},\boldsymbol{\xi})\right]u^n(\boldsymbol{x})\end{pmatrix}\times d\Gamma(\boldsymbol{x})+u^{ff.N}(\boldsymbol{\xi}) \tag{4}$$

where $u^n(\boldsymbol{x})$ and $q^n(\boldsymbol{x})$ are displacement and traction fields, respectively; $u^{ff.N}$ stands for the free field displacement at time $t=N\,\Delta t$; and $U_1^{N-n+1}(\boldsymbol{x},\boldsymbol{\xi})+U_2^{N-n}(\boldsymbol{x},\boldsymbol{\xi})$ and $Q_1^{N-n+1}(\boldsymbol{x},\boldsymbol{\xi})+Q_2^{N-n}(\boldsymbol{x},\boldsymbol{\xi})$ denote the half-plane displacement and traction time-convoluted kernels, respectively. These closed-form responses can be found in Panji et al. [53] and Panji et al. [68]. All the processes were completely analytically carried out up to now. After discretizing the necessary boundaries of the body by M quadratic elements, spatial integration can be numerically

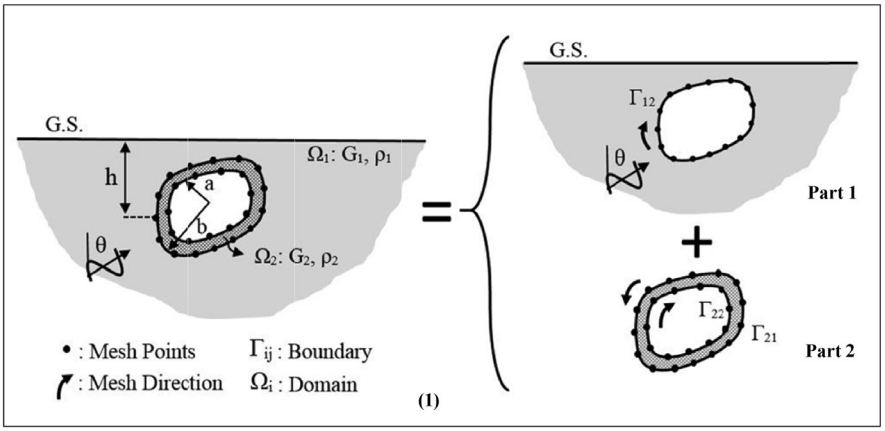

Fig. 1. A definition sketch for solving the lined tunnel problems using half-plane time-domain BEM approach.

done as follows:

$$c(\xi)u^N(\xi) = \sum_{n=1}^{N}\sum_{m=1}^{M} \times\left[\begin{Bmatrix}\int_{\Gamma_m}\left[U_1^{N-n+1}(\boldsymbol{x}(\kappa),\xi)+U_2^{N-n}(\boldsymbol{x}(\kappa),\xi)\right]N_\alpha(\kappa)|J|\,d\kappa\end{Bmatrix}q_\alpha^n - \begin{Bmatrix}\int_{\Gamma_m}\left[Q_1^{N-n+1}(\boldsymbol{x}(\kappa),\xi)+Q_2^{N-n}(\boldsymbol{x}(\kappa),\xi)\right]N_\alpha(\kappa)|J|\,d\kappa\end{Bmatrix}u_\alpha^n\right] + u^{ff.N}(\xi) \tag{5}$$

in which M represents the total number of boundary elements, Γ_m stands for the portion of the boundary to which element "m" belongs, $N_\alpha(\kappa)$ denotes quadratic shape functions in terms of the local intrinsic coordinates of κ ($\alpha = 1,\ 2,\ 3$), and J indicates the Jacobian of transformation. With the help of regular Gauss quadrature and special logarithmic integration for nonsingular and singular integrals, respectively, the following matrix form can be obtained for BIE [73]:

$$\sum_{n=1}^{N}\boldsymbol{H}^{N-n+1}\{\boldsymbol{u}^n\} = \sum_{n=1}^{N}\boldsymbol{G}^{N-n+1}\{\boldsymbol{q}^n\} + \{\boldsymbol{u}^{ff.N}\} \tag{6}$$

where $\boldsymbol{H}^{N-n+1}$ and $\boldsymbol{G}^{N-n+1}$ are the matrices obtained from the integration over BEs; $\{\boldsymbol{u}^n\}$ and $\{\boldsymbol{q}^n\}$ are vectors of boundary nodal quantities; and $\{\boldsymbol{u}^{ff.N}\}$ is a matrix including free field displacements. After applying boundary conditions over all the nodes, the solvable form of Eq. (6) can be obtained as follows:

$$[\boldsymbol{A}_1^1]\{\boldsymbol{X}^N\} = [\boldsymbol{B}_1^1]\{\boldsymbol{Y}^N\} + \{\boldsymbol{R}^N\} + \{\boldsymbol{u}^{ff.N}\} \tag{7}$$

where $\{\boldsymbol{X}^N\}$ and $\{\boldsymbol{Y}^N\}$ are vectors of unknown and known boundary quantities, respectively, and $[\boldsymbol{A}_1^1]$ and $[\boldsymbol{B}_1^1]$ are matrices corresponding to the above vectors. $\{\boldsymbol{R}^N\}$ denotes the effects of past dynamic history on the current time node N, presented as follows:

$$\{\boldsymbol{R}^N\} = \sum_{n=1}^{N-1}\left(\boldsymbol{G}^{N-n+1}\{\boldsymbol{q}^n\} - \boldsymbol{H}^{N-n+1}\{\boldsymbol{u}^n\}\right) \tag{8}$$

3.3. Internal points

After solving Eq. (7), all unknown boundary quantities can be achieved. To obtain the responses on the smooth ground surface, the geometric coefficient of $c(\xi)$ in Eq. (3) must be assumed equal to 1. As can be observed in Fig. 1, smooth ground surface belongs to Domain 1. Thus, internal points must be placed in the equations related to this domain.

4. Modeling

As can be seen in Fig. 1, the model is assembled from an unlined cavity embedded in a half-plane and a closed ring-shaped medium. After discretizing all the required boundaries (e.g. interface and inner boundary around the tunnel) and using half-plane time-domain BEM presented above for each domain, all matrices can be obtained to form the BIEs. Finally, coupled equations can be illustrated by applying continuity and boundary conditions.

4.1. Part 1: A pitted half-plane

This domain of the model is a two-dimensional half-space medium with an embedded arbitrarily shaped unlined cavity subjected to propagating obliquely incident SH-waves, as shown in Fig. 1. The ground surface and seismic waves belong to this part of the model. The boundary of the cavity is actually the interface of the lining with the surrounding domain. The discretization must be done clockwise in order to define the normal vector towards the inside. After discretizing the cavity (denoted by subscript 12) and performing its BIE, the following matrix equation for time step $N = n$ can be obtained as

$$\left[\boldsymbol{H}_{12}^1\right]\left\{\boldsymbol{u}_{12}^N\right\} = \left[\boldsymbol{G}_{12}^1\right]\left\{\boldsymbol{q}_{12}^N\right\} + \left\{\boldsymbol{R}_{12}^N\right\} + \left\{\boldsymbol{u}_{12}^{ff.N}\right\} \tag{9}$$

in which:

$$\left\{\boldsymbol{R}_{12}^N\right\} = \sum_{n=1}^{N-1}\left(\boldsymbol{G}_{12}^{N-n+1}\left\{\boldsymbol{q}_{12}^n\right\} - \boldsymbol{H}_{12}^{N-n+1}\left\{\boldsymbol{u}_{12}^n\right\}\right) \tag{10}$$

where $\boldsymbol{u}_{12}^N$ and $\boldsymbol{q}_{12}^N$ are displacements and tractions at the interface for part 1, respectively; $\boldsymbol{R}_{12}^N$ is past dynamic history on current time node N; and $\boldsymbol{u}_{12}^{ff.N}$ indicates free field displacements for the interface nodes which are in fact the input motion of the problem.

4.2. Part 2: A closed ring-shaped medium

This part is the lining as a ring-shaped medium including two closed boundaries, one inner and other outer boundary or the interface. To define the normal vector in the correct direction, a discretization must be done clockwise and counter clockwise for the inner boundary and the interface, respectively. Although ring-shaped medium is embedded in a half-plane as demonstrated in Fig. 1, the ground surface and seismic waves are absent in this part of the model. Therefore, free field displacements cannot be seen in the obtained equations ($\boldsymbol{u}^{ff}$). After discretizing the model, forming the considered matrices, and differentiating the nodes at the inner boundary (denoted by subscript 2) from those on the interface (denoted by subscript 21), the matrix form of BIE for time step

$N=n$ can be obtained as

$$\begin{bmatrix} \boldsymbol{H}_{21}^{1} & \boldsymbol{H}_{2}^{1} \end{bmatrix} \begin{Bmatrix} \boldsymbol{u}_{21}^{N} \\ \boldsymbol{u}_{2}^{N} \end{Bmatrix} = \begin{bmatrix} \boldsymbol{G}_{21}^{1} & \boldsymbol{G}_{2}^{1} \end{bmatrix} \begin{Bmatrix} \boldsymbol{q}_{21}^{N} \\ \boldsymbol{q}_{2}^{N} \end{Bmatrix} + \begin{Bmatrix} \boldsymbol{R}_{21}^{N} \\ \boldsymbol{R}_{2}^{N} \end{Bmatrix} \tag{11}$$

in which:

$$\left\{ \boldsymbol{R}_{21}^{N} \right\} = \sum_{n=1}^{N-1} \left(\boldsymbol{G}_{21}^{N-n+1} \left\{ \boldsymbol{q}_{21}^{n} \right\} - \boldsymbol{H}_{21}^{N-n+1} \left\{ \boldsymbol{u}_{21}^{n} \right\} \right) \tag{12}$$

and

$$\left\{ \boldsymbol{R}_{2}^{N} \right\} = \sum_{n=1}^{N-1} \left(\boldsymbol{G}_{2}^{N-n+1} \left\{ \boldsymbol{q}_{2}^{n} \right\} - \boldsymbol{H}_{2}^{N-n+1} \left\{ \boldsymbol{u}_{2}^{n} \right\} \right) \tag{13}$$

where $\boldsymbol{u}_{21}^{N}$ and $\boldsymbol{q}_{21}^{N}$ are displacements and tractions at the interface nodes of part 2, respectively; $\boldsymbol{u}_{2}^{N}$ and $\boldsymbol{q}_{2}^{N}$ are displacements and tractions on the inner boundary of the lining, respectively; and $\boldsymbol{R}_{21}^{N}$ and $\boldsymbol{R}_{2}^{N}$ denote past dynamic history for the interface and inner surface of the lining, respectively.

4.3. Assembling

After determining the discretized BIEs for each part, two series equations must be assembled into a coupled equation for simultaneous solution. For this purpose, continuity conditions must be applied at the interface. By considering these conditions, we can write:

$$\boldsymbol{u}_{12}^{N} = \boldsymbol{u}_{21}^{N} \tag{14}$$

$$\mu_1 \, \boldsymbol{q}_{12}^{N} = -\mu_2 \, \boldsymbol{q}_{21}^{N} \tag{15}$$

where μ_1 and μ_2 are shear modules for half-plane and the lining, respectively. According to Eqs. (14) and (15), with the displacements being equalized and the tractions being vanished at the interface, the original coupled equation can be obtained as follows:

$$\begin{bmatrix} \boldsymbol{H}_{12}^{1} & 0 & -\frac{1}{\mu_1}\boldsymbol{G}_{12}^{1} \\ \boldsymbol{H}_{21}^{1} & \boldsymbol{H}_{2}^{1} & \frac{1}{\mu_2}\boldsymbol{G}_{21}^{1} \end{bmatrix} \begin{Bmatrix} \boldsymbol{u}_{12}^{N} \\ \boldsymbol{u}_{2}^{N} \\ \boldsymbol{q}_{12}^{N} \end{Bmatrix} = \begin{bmatrix} 0 & \boldsymbol{G}_{2}^{1} \end{bmatrix} \begin{Bmatrix} 0 \\ \boldsymbol{q}_{2}^{N} \end{Bmatrix} + \begin{Bmatrix} \boldsymbol{R}_{12}^{N} \\ \boldsymbol{R}_{(2)}^{N} \end{Bmatrix} + \begin{Bmatrix} \boldsymbol{u}_{12}^{ff.N} \\ 0 \end{Bmatrix} \tag{16}$$

in which:

$$\boldsymbol{R}_{(2)}^{N} = \begin{Bmatrix} \boldsymbol{R}_{21}^{N} \\ \boldsymbol{R}_{2}^{N} \end{Bmatrix} \tag{17}$$

Given that stress-free boundary conditions occur on the inner surface of the lining, $\boldsymbol{q}_{2}^{N}$ is also equal to zero. Therefore, after applying these conditions, the following equation can be written:

$$\begin{bmatrix} \boldsymbol{H}_{12}^{1} & 0 & -\frac{1}{\mu_1}\boldsymbol{G}_{12}^{1} \\ \boldsymbol{H}_{21}^{1} & \boldsymbol{H}_{2}^{1} & \frac{1}{\mu_2}\boldsymbol{G}_{21}^{1} \end{bmatrix} \begin{Bmatrix} \boldsymbol{u}_{12}^{N} \\ \boldsymbol{u}_{2}^{N} \\ \boldsymbol{q}_{12}^{N} \end{Bmatrix} = \begin{Bmatrix} \boldsymbol{R}_{12}^{N} \\ \boldsymbol{R}_{(2)}^{N} \end{Bmatrix} + \begin{Bmatrix} \boldsymbol{u}_{12}^{ff.N} \\ 0 \end{Bmatrix} \tag{18}$$

The above equation can be directly solved to obtain the unknown values at the interface as well as the displacements at the inner boundary of the lining. Once all boundary values are determined, the displacements on the smooth ground surface can be achieved as internal points. According to Section 3.3, to obtain the responses on the ground surface, the discretized BIE for an internal point m can be modified as follows:

$$\left\{ \boldsymbol{u}^{N\cdot m} \right\} = \sum_{n=1}^{N} \left(\left[\frac{1}{\mu_1} \boldsymbol{G}_{12}^{\langle N-n+1\cdot m \rangle} \right] \left\{ \boldsymbol{q}_{12}^{n} \right\} \right) - \sum_{n=1}^{N} \left(\left[\boldsymbol{H}_{12}^{\langle N-n+1\cdot m \rangle} \right] \left\{ \boldsymbol{u}_{12}^{n} \right\} \right) + \left\{ \boldsymbol{u}^{ff\cdot N\cdot m} \right\} \tag{19}$$

where $\boldsymbol{u}^{N.m}$ and $\boldsymbol{u}^{ff.N.m}$ are the displacement and the free field motion at internal points, respectively, and $\boldsymbol{G}_{12}^{\langle N-n+1.m \rangle}$ and $\boldsymbol{H}_{12}^{\langle N-n+1.m \rangle}$ are the matrices in which the elements are obtained by considering the internal points and boundary nodes as source and receiver points, respectively.

5. Validation example

The above formulation was implemented in a developed BEM algorithm, previously called as DASBEM [53]. To validate the formulation as well as the prepared code in modeling the lined tunnels, a practical example was analyzed and compared with those of the published works. In this regard, the Ricker wavelet function was considered as the input motion [76]. To satisfy stress-free boundary conditions on the smooth ground surface, the Ricker function was presented in two parts according to incident and reflected waves as follows:

$$u^{ff}(x,y,t) = a_{\max} \cdot \begin{pmatrix} \left[1 - 2\left(\frac{\pi f_p}{c} \alpha^{\text{inc.}} \right)^2 \right] e^{-\left(\frac{\pi f_p}{c} \alpha^{\text{inc.}} \right)^2} H\left(t - \frac{r^{\text{inc.}}}{c} \right) \\ + \left[1 - 2\left(\frac{\pi f_p}{c} \alpha^{\text{ref.}} \right)^2 \right] e^{-\left(\frac{\pi f_p}{c} \alpha^{\text{ref.}} \right)^2} H\left(t - \frac{r^{\text{ref.}}}{c} \right) \end{pmatrix} \tag{20}$$

in which:

$$\alpha^{\text{inc.}} = c\,(t - t_0) + r^{\text{inc.}};\; r^{\text{inc.}} = -\sin\theta.x + \cos\theta.y \tag{21}$$

and

$$\alpha^{\text{ref.}} = c\,(t - t_0) + r^{\text{ref.}};\; r^{\text{ref.}} = -\sin\theta.x - \cos\theta.y \tag{22}$$

where f_p, t_0 and $a_{\max}$ are predominant frequency, time-shift parameter, and maximum displacement time-history, respectively; $H(.)$ is the Heaviside function; θ is the incident wave angle; and $\alpha^{\text{inc.}}$ and $\alpha^{\text{ref.}}$ are the phase of incident and reflected waves, respectively. In Fig. 2, the dimensionless shape of the Ricker wavelet time history is presented for an assumed point on the regular ground surface. Because of having a unit dominant pulse, this form of incident waves is favorable in numerical models.

5.1. Circular unlined tunnel

A circular lined tunnel was modeled as the unlined case. In this regard, material properties of the lining were equal to those of the surrounding domain. A half-plane including an embedded circular cavity subjected to SH-waves was analyzed by Lee [3] and Luco and de barros [49] using an analytical approach and the full-plane frequency-domain BEM, respectively. To this end, the tunnel was buried in the depth of 1.5 b. The inner radius (a) and thickness of the lining (t) were assumed equal to 200 m and 0.1 b, respectively. The characteristics of the Ricker wavelet, i.e. maximum amplitude, time-shift parameter, and predominant frequency, were equal to 0.001 m, 1.4 s, and 3 Hz, respectively. The boundaries (i.e. inner boundary of the lining and the interface) were discretized with 80 elements, and 121 internal points were considered on the smooth ground surface. The problem was analyzed by 500 time steps with the time interval of 0.01 s. The density and shear wave velocity of the surrounding domain which were equal to lining properties were included as 1 ton/m^3 and 800 m/s, respectively. To present the results, the dimensionless frequency must be defined as follows:

$$\eta = \frac{\omega\, b}{\pi\, c} \tag{23}$$

in which η is the dimensionless frequency, ω is the angular frequency, and c is the shear wave velocity. Fig. 3 depicts the normalized displacement amplitude ($|u|$) of the ground surface in the presence of an embedded lined tunnel including the same materials as those of the surrounding domain subjected to vertically propagating incident plane SH-waves in the dimensionless frequencies of 0.5 to 1.5, respectively. The normalized displacement amplitude was defined as the ratio of ground surface displacement amplitude to input motion amplitude. As can be observed,

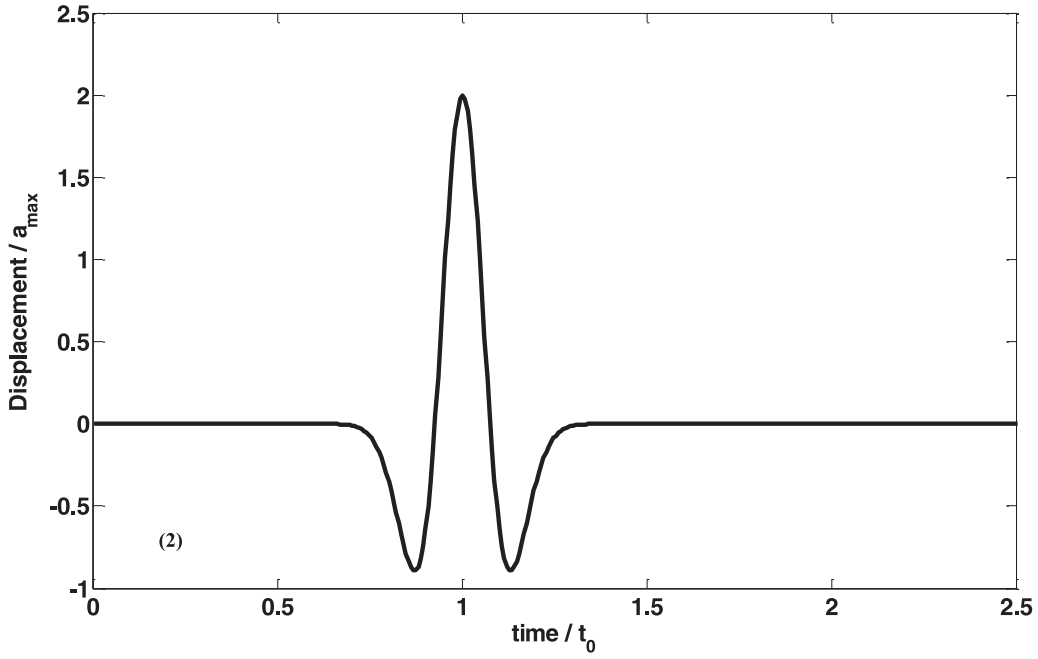

Fig. 2. Displacement time history of the Ricker wavelet.

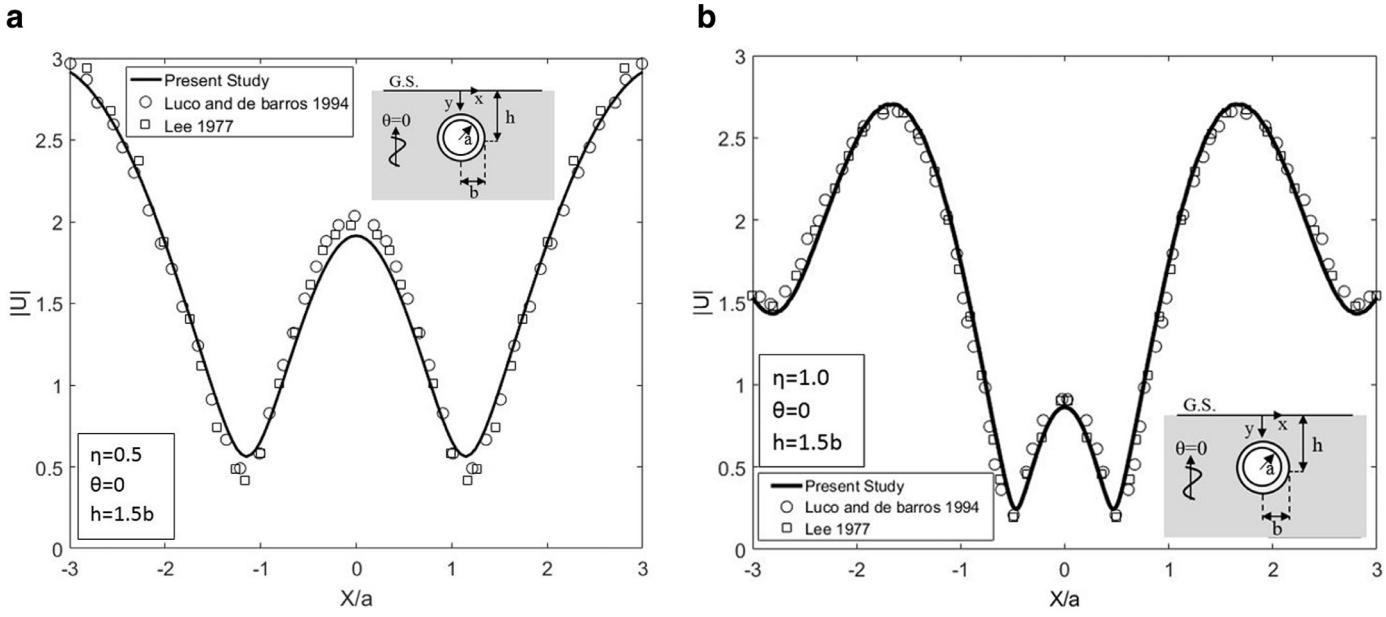

Fig. 3. Normalized displacement amplitude of the ground surface in the presence of a circular lined tunnel with material properties equal to those of the surrounding domain subjected to vertical incident SH-waves.

the responses are in agreement with those of solutions presented by Lee [3] and Luco and de barros [49].

6. Numerical results

To demonstrate the ability of the present approach for modeling actual problems, a circular tunnel with concrete lining was assumed in a half-plane including silty clay soil. Although this problem was solved in the literature ([8, 10, 24]), presenting surface responses at high frequencies and obtaining some developed results are the main purposes of this section. The properties of the lining and the soil are shown in Table 1 [9]. If the impedance ratio (I) of the two domains were define as follows:

$$I = \frac{(\rho\, c)_{\text{soil}}}{(\rho\, c)_{\text{lining}}} \tag{24}$$

then, according to the assumed properties, it would be obtained equal to 0.10 in this problem. This means that the lining was about ten times harder than its surrounding domain. To achieve favorable responses, the boundaries of tunnel were discretized with 59 BEs. A total of 121 internal points was located in the surface. The depths of 1.5 b and 2.5 b were considered for the tunnel. The dimensionless thickness of lining was equal to 0.1 b. Four angles of the incident wave were applied as 0, 30, 60, and 90°. Depending on the depth of the tunnel, the

Table 1
Properties of the soil and the lining for numerical example.

	Density (ton/m^3), ρ	Shear wave velocity (m/s), c	Shear modulus (GPa), μ
Properties of the soil	1.64	275	0.124
Properties of the lining	2.41	1870	8.40

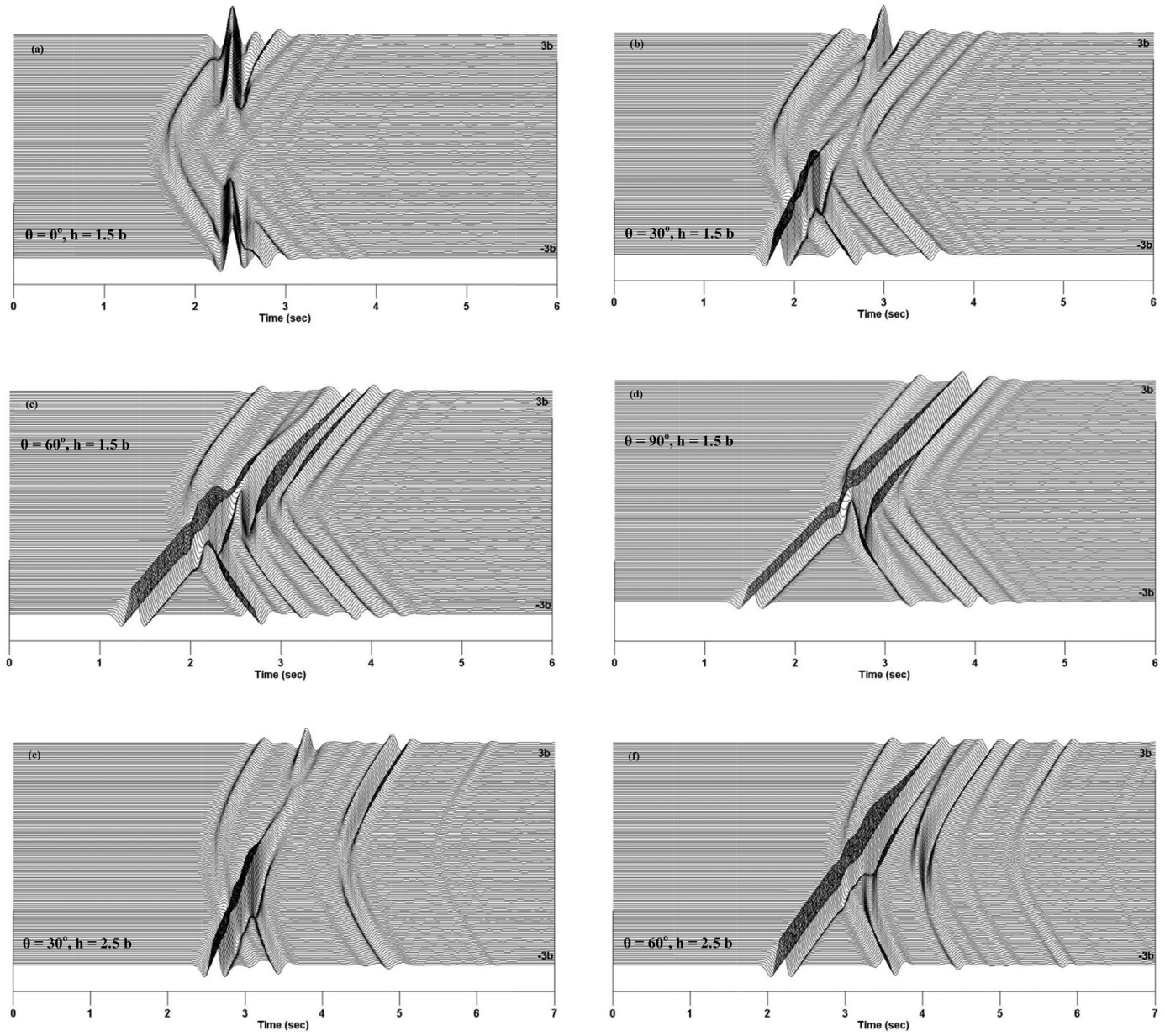

Fig. 4. Synthetic seismograms of the surface in the presence of a circular lined tunnel in the depth of h and incident SH-wave angle of θ (a) h = 1.5 b, $\theta = 0^\circ$ (b) h = 1.5 b, $\theta = 30^\circ$ (c) h = 1.5 b, $\theta = 60^\circ$ (d) h = 1.5 b, $\theta = 90^\circ$ (e) h = 2.5 b, $\theta = 30^\circ$ (f) h = 2.5 b, $\theta = 60^\circ$.

time-shift parameter of the Ricker wavelet and the number of time steps were changed from 2.4 to 4.4 s and 600–800, respectively. Other parameters were the same as those of previous example.

6.1. Synthetic seismograms

In the time-domain analysis, synthetic seismograms can be directly obtained. Fig. 4 illustrates the synthetic seismograms of the surface in the presence of a circular lined tunnel embedded in the depths of 1.5 b and 2.5 b subjected to incident SH-waves with different angles. In the case of the vertical incident wave (Fig. 4(a)), the reflection and refraction of the waves are low compared to oblique incident cases, and the responses converge rapidly. As can be seen in Fig. 4(b)–(d), for the angles of 30°, 60°, and 90°, not only are the effect of creeping and reflected waves more obvious, but also the amplitude of the responses are greater than those of the vertical case, especially near the wave front. With increasing the depth of the tunnel, a distance is created between the waves reflected from the surface. Fig. 4(e) and (f) presents synthetic seismograms for a lined tunnel in the depth of 2.5 b under incident SH-waves with the angle of 30° and 60°, respectively. As can be seen, by creating

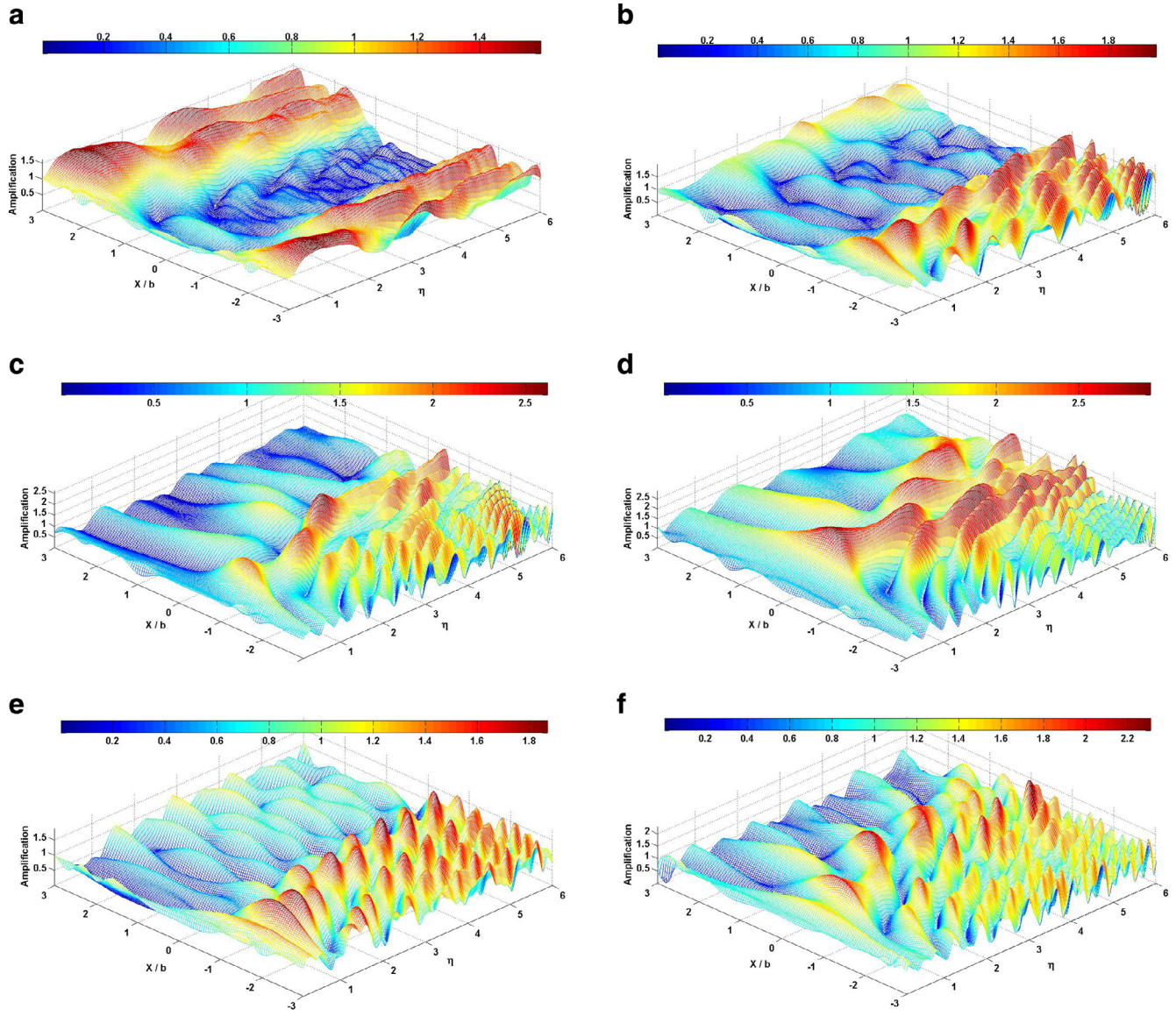

Fig. 5. 3D amplification of the surface in the presence of a circular lined tunnel in the depth of h and incident SH-wave angle of θ (a) $h = 1.5$ b, $\theta = 0^\circ$ (b) $h = 1.5$ b, $\theta = 30^\circ$ (c) $h = 1.5$ b, $\theta = 60^\circ$ (d) $h = 1.5$ b, $\theta = 90^\circ$ (e) $h = 2.5$ b, $\theta = 30^\circ$ (f) $h = 2.5$ b, $\theta = 60^\circ$.

the distance between the reflected waves, the convergence occurs later than the corresponding case in the depth of 1.5 b, and the amplitudes are reduced. It seems that seismograms are stretched with increasing the depth.

6.2. Frequency-domain responses

The amplitudes of responses can be obviously observed in the frequency domain. Thus, three-dimensional frequency-domain responses are presented in Fig. 5. This figure shows the amplification (the ratio of ground response amplitude to the free-filed case) of the surface versus the dimensionless frequencies for a circular lined tunnel subjected to oblique incident SH-waves. As can be seen in Fig. 5(a), the presence of lined tunnel has a mitigating role for vertical incident waves in the upper range of the tunnel, so that even de-amplification increases with increasing the frequency. Nevertheless, in the cases of oblique waves (Fig. 5(b)-(d)), the performance is observed differently. A safe region forms beyond the tunnel away from wave front. The responses swing slowly around the free field. Maximum amplification is illustrated at the edge of the tunnel near the wave front on the surface. Although fluctuations increase with growing the depth (Fig. 5(e) and (f)), the amplitudes reduce in the side near the wave front.

6.3. Twin lined tunnels

To show the practicability of the present method as well as the efficiency of the developed algorithm, an example was analyzed including the interaction of twin circular lined tunnels subjected to propagating incident SH-wave. Schematic drawing of the example with all parameters is shown in Fig. 6. All parameters were the same as those of previous example. It was assumed that the material properties of two linings were the same. As can be seen in Fig. 6, only the boundaries around the tunnels were discretized to create the model. Fig. 7(a) and (b) shows the synthetic seismograms of the surface in the presence of two circular lined tunnels embedded in the depth of 1.5 b at distance of 2.5 b subjected to propagating incident SH-wave with angles of 0° and 90°, respectively. The results are presented in the range of −5 b to 5 b from the smooth surface. As can be seen, the interaction effect of twin tunnels are obtained on the responses compared to single tunnel (Fig. 4(a) and (d)). In these figures, the trapped waves as well as high fluctuations of

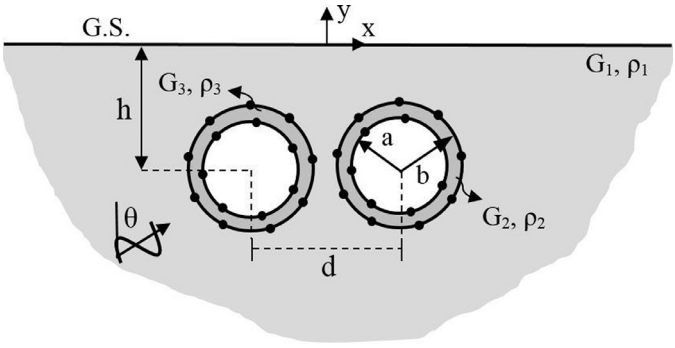

Fig. 6. Schematic drawing of the twin circular lined tunnels subjected to incident SH-wave.

the responses are obvious. Also, multiple diagonal ridges can be seen on the responses due to the reflection of the waves between the ground surface and tunnels crest. It is obvious that the responses are reduced by increasing the distance between tunnels. As can be seen in Fig. 7(c), for the tunnels in the distance of 3 b, not only the wave oscillations but also the amplitude of the responses are slower than case of 2.5 b. Fig. 7(d)–(f) presents the synthetic seismograms of the surface for the tunnels embedded in the depth of 2.5 b and distances of 2.5 b, 3 b and 4 b, respectively. In this depth, increasing the distance between the tunnels has more influence to reduce the responses compared to the previous case.

In Fig. 8(a)–(f), three-dimensional amplification pattern of the ground surface can be observed in the presence of twin circular lined tunnels in different depths and distances. As can be seen, de-amplification pattern are frequently observed on the surface above the tunnels in the case of vertical incident SH-wave. There are always critical responses between two tunnels on the surface. With increasing the depth of the tunnels, the responses of the sides of the ground surface are also amplified. But, the distance between the tunnels has a different effect, so that de-amplification ranges (or seismic isolated areas) are increased by increasing the distance between two tunnels. It is obvious that the depth and distance of the tunnels are affected on the formation of response patterns.

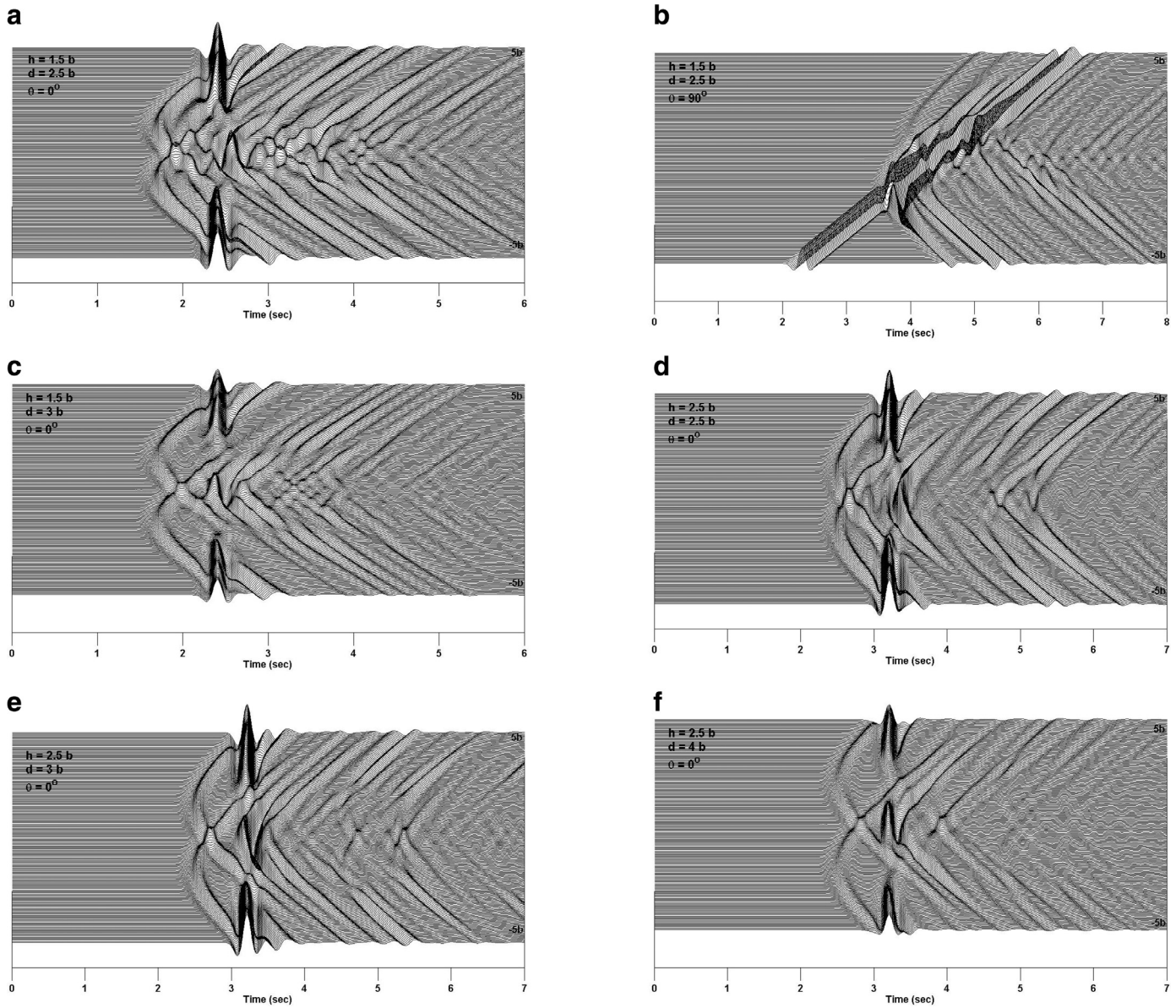

Fig. 7. Synthetic seismograms of the surface in the presence of twin circular lined tunnels (a) $h = 1.5$ b, $d = 2.5$ b, $\theta = 0^\circ$ (b) $h = 1.5$ b, $d = 2.5$ b, $\theta = 90^\circ$ (c) $h = 1.5$ b, $d = 3$ b, $\theta = 0^\circ$ (d) $h = 2.5$ b, $d = 2.5$ b, $\theta = 0^\circ$ (e) $h = 2.5$ b, $d = 3$ b, $\theta = 0^\circ$ (f) $h = 2.5$ b, $d = 4$ b, $\theta = 0^\circ$.

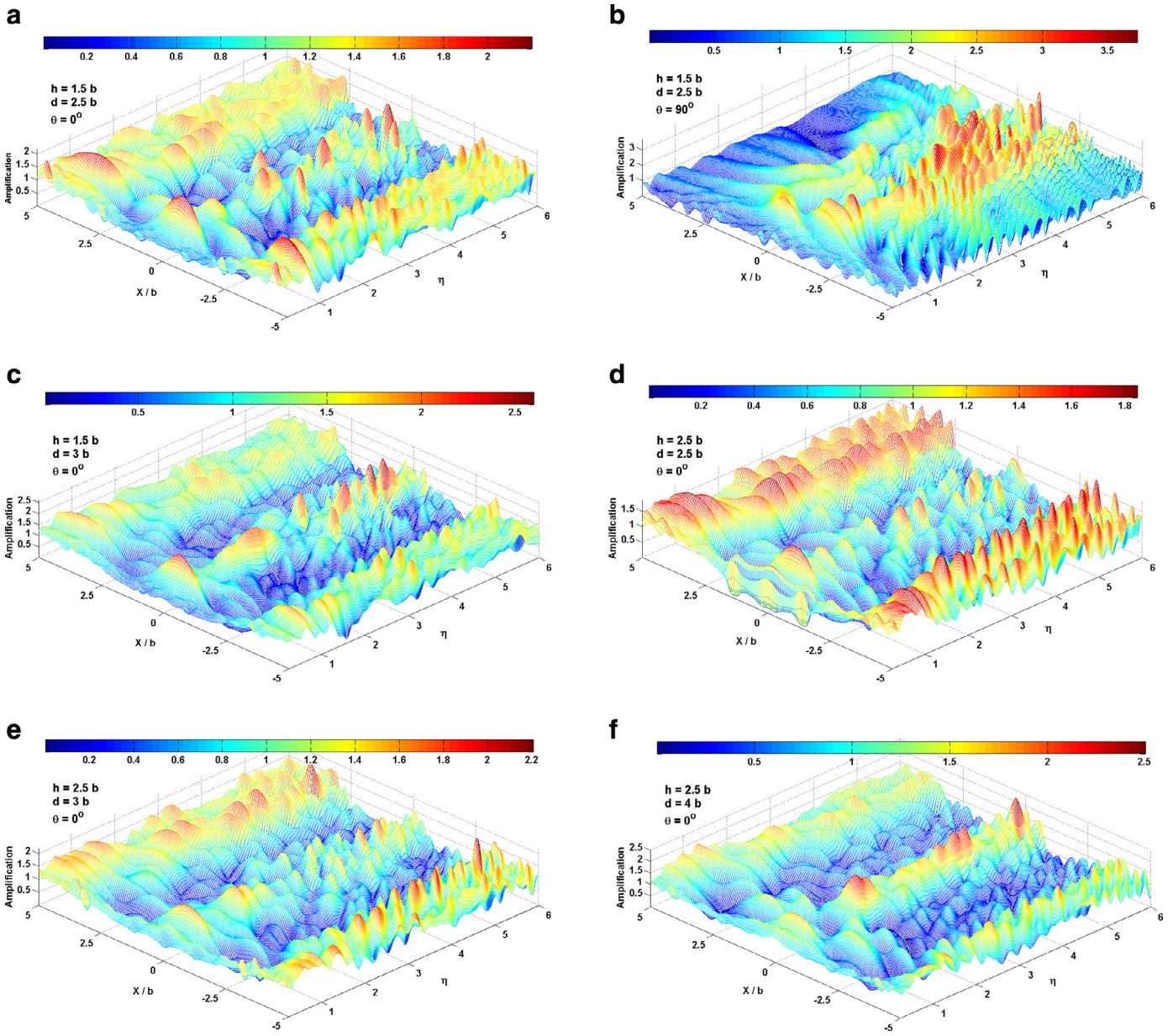

Fig. 8. 3D amplification of the surface in the presence of twin circular lined tunnels (a) $h = 1.5$ b, $d = 2.5$ b, $\theta = 0^\circ$ (b) $h = 1.5$ b, $d = 2.5$ b, $\theta = 90^\circ$ (c) $h = 1.5$ b, $d = 3$ b, $\theta = 0^\circ$ (d) $h = 2.5$ b, $d = 2.5$ b, $\theta = 0^\circ$ (e) $h = 2.5$ b, $d = 3$ b, $\theta = 0^\circ$ (f) $h = 2.5$ b, $d = 4$ b, $\theta = 0^\circ$.

7. Conclusions

An advanced half-plane time-domain BEM approach was developed and successfully applied to analyze a homogeneous elastic two-dimensional half-space including arbitrarily shaped embedded lined tunnels subjected to propagating incident SH-waves. Utilization of this approach only required the discretization of the tunnels. The model was established based on a decomposition scenario as the interaction between a pitted half-plane and a ring-shaped domain. After computing the influence coefficients of matrices for each domain and satisfying the continuity and boundary conditions, respectively, at the interface and inner boundary of tunnel, a coupled equation was obtained for the step-by-step analysis in the time domain. This process was properly implemented in developing a known temporal algorithm which had previously been called as DASBEM [53,68,69]. To demonstrate the ability of the approach as well as the efficiency of the algorithm, an example was analyzed and compared with those of the published works. The results indicated that the method has a favorable accuracy for solving lined tunnel problems. Moreover, a practical example was investigated to illustrate the extensive numerical results of single/twin circular concrete lined tunnels buried in the soft soil subjected to propagating oblique incident SH-waves at high frequencies. In this regard, some effective parameters were considered on the amplification pattern of the ground surface, whose results can be summarized as follows:

1- Synthetic seismograms indicate that increasing the angle of incident has a positive effect on the refraction of the waves and spread of the reflected waves' region.
2- Three-dimensional frequency-domain responses showed that the presence of the lined tunnel against vertical waves was more efficient in reducing surface amplification at different frequencies compared to other cases of incident. Also, it was seen that forming the safe area can be obtained in the opposite side of the wave front for propagating oblique waves, especially in a shallow depth.

3- The depth of the tunnel establishment affected the form of the response pattern. Increasing the depth reduced not only the amplitudes, but also the number of oscillations in the case of vertical incident.
4- Synthetic seismograms of the surface for twin lined tunnel show that the distance between the tunnels has important influence on the response formation, especially on its concentration and the distribution of oblique ridges.
5- By increasing the distance between two tunnels, de-amplification areas were increased on the surface not only the above the tunnels, but also on both sides in vertical incident case.

Although this paper was focused on the displacement factor as well as amplification ratio of the ground surface, obtaining the stress concentration factor around the lined tunnels using the proposed method is an interesting topic, which will be presented in the future works.

Acknowledgment

The authors would like to express their gratitude to the respected editor-in-chief, Prof. Alexander H.-D. Cheng, and two anonymous reviewers for their useful comments and precious time spent on our paper.

References

[1] Ariman T, Muleski GE. A review of the response of buried pipelines under seismic excitations. Earthq Eng Struct Dyn 1981;9:133–51.
[2] Panji M. Seismic analysis of topographic features due to propagating incident SH-waves by half-plane time-domain BEM, [Ph.D. Dissertation]. Tehran, Iran: Islamic Azad University, Science and Research Branch; 2013.
[3] Lee VW. On the deformations near circular underground cavity subjected to incident plane SH-waves. In: Proceedings of symposium of applications of computer methods in engineering conference. Los Angeles: University of Southern California; 1977. p. 951–62.
[4] Datta SK, Shah AH. Scattering of SH waves by embedded cavities. Wave Mot 1982;4:265–83.
[5] Lee VW, Chen S, Hsu IR. Antiplane diffraction from canyon above subsurface unlined tunnel. J Eng Mech 1999;125(6):668–75.
[6] Tsaur DH, Chang KH. Multiple scattering of sh waves by an embedded truncated circular cavity. J Marine Sci Technol 2012;20(1):73–81.
[7] Gao Y, Dai D, Zhang N, Wu Y, Mahfouz AH. Scattering of plane and cylindrical sh waves by a horseshoe shaped cavity. J Earthq Tsunami 2016;10(2):1–23.
[8] Lee VW, Trifunac MD. Response of tunnels to incident SH waves. J Eng Mech Div 1979;105(4):643–59.
[9] Balendra T, Thambiratnam DP, Koh CG, Lee SL. Dynamic response of twin circular tunnels due to incident SH-waves. Earthq Eng Struct Dyn 1984;12:181–201.
[10] Smerzini C, Aviles J, Paolucci R, Sanchez-Sesma FJ. Effect of underground cavities on surface earthquake ground motion under SH wave propagation. Earthq Eng Struct Dyn 2009;38(12):1441–60.
[11] Zhang Y, Zhou C, Liu Y. Dynamic stresses concentrations of SH wave by circular tunnel with lining. Adv Mater Res 2011;323:18–22.
[12] Li YS, Li TB, Zhang X. Response of shallow–buried circular lining tunnel to incident P wave. Appl Mech Mater 2012;160:331–6.
[13] Min H, Bing-Yu P. Dynamic stress concentration of underground lined cavities in different distance under incident plane SV wave. Adv Mater Res 2012;446–449:2317–20.
[14] Liu Q, Zhao M, Wang L. Scattering of plane P, SV or rayleigh waves by a shallow lined tunnel in an elastic half space. Soil Dyn Earthq Eng 2013;49:52–63.
[15] Xu H, Li T, Xu J, Wang Y. Dynamic response of underground circular lining tunnels subjected to incident P waves. Math Probl Eng 2014;2014:1–11.
[16] Yi C, Zhang P, Johansson D, Nyberg U. Dynamic analysis for a circular lined tunnel with an imperfectly bonded interface impacted by plane SH-waves. In: Proceeding of the Word Tunnel Congress. Brazil; 2014. p. 1–7.
[17] Shi S, Han F, Wang Z, Liu D. The interaction of plane SH-waves and non-circular cavity surfaced with lining in anisotropic media. Appl Math Mech 1996;17(9):855–67.
[18] Hasheminejad SM, Kazemirad S. Dynamic response of an eccentrically lined circular tunnel in poroelastic soil under seismic excitation. Soil Dyn Earthq Eng 2008;28:277–92.
[19] Jiang L-F, Zhou X-L, Wang J-H. Scattering of a plane wave by a lined cylindrical cavity in a poroelastic half-space. Comput Geotech 2009;36:773–86.
[20] Datta SK, Shah AH, Wong KC. Dynamic stresses and displacements in buried pipe. J Eng Mech 1984;110:1451–66.
[21] Wong KC, Shah AH, Datta SK. Dynamic stresses and displacements in a buried tunnel. J Eng Mech 1985;111:218–34.
[22] Chin YF, Rajapakse RKND, Shah AH, Datta SK. Dynamics of buried pipes in back–filled trench. Soil Dyn Earthq Eng 1987;6(3):158–63.
[23] Moore ID, Guan F. Three-dimensional dynamic response of lined tunnels due to incident seismic waves. Earthq Eng Struct Dyn 1996;25:357–69.
[24] Manoogian ME. Scattering and diffraction of SH waves above an arbitrarily shaped tunnel. ISET J Earthq Technol 2000;37(1-3):11–26.
[25] Davis CA, Lee VW, Bardet JP. Transverse response of underground cavities and pipes to incident SV waves. Earthq Eng Struct Dyn 2001;30:383–410.
[26] Yeh C-S, Teng T-J, Shyu W-S, Tsai I-C. A hybrid method for analyzing the dynamic responses of cavities or shells buried in an elastic half-plane. J Mech 2002;18(2):75–87.
[27] Liao W-I, Yeh C-S, Teng T-J. Scattering of elastic waves by a buried tunnel under obliquely incident waves using T matrix. J Mech 2008;24(4):405–18.
[28] Liu Z, Wang Y, Liang J. Dynamic interaction of twin vertically overlapping lined tunnels in an elastic half space subjected to incident plane waves. Earthq Sci 2016;29(3):185–201.
[29] Zhou X-L, Wang J-H, Jiang L-F. Dynamic response of a pair of elliptic tunnels embedded in a poroelastic medium. J Sound Vib 2009;325:816–34.
[30] Besharat V, Davoodi M, Jafari MK. Effect of underground structures on free-field ground motion during earthquakes. In: Proceedings of the fifteenth world conference on earthquake engineering, Lisbon, Portugal; 2012.
[31] Esmaeili M, Vahdani S, Noorzad A. Dynamic response of lined tunnel to plane harmonic waves. Tunnel Undergr Space Technol 2006;21:511–19.
[32] Faccioli E, Maggio F, Paolucci R, Quarteroni A. 2D and 3D elastic wave propagation by a pseudo-spectral domain decomposition method. J Seismol 1997;1:237–51.
[33] Gelagoti F, Kourkoulis R, Anastapoulos I, Gazetas G. Nonlinear dimensional analysis of trapezoidal valleys subjected to vertically propagating sv waves. Bull Seismol Soc Am 2012;102(3):999–1017.
[34] Huang J-Q, Du X-L, Jin L, Zhao M. Impact of incident angles of P waves on the dynamic response of long lined tunnels. Earthq Eng Struct Dyn 2016;45(15):2435–54.
[35] Narayan JP, Kumar D, Sahar D. Effects of complex interaction of rayleigh waves with tunnel on the free surface ground motion and the strain across the tunnel-lining. Nat Haz 2015;79(1):479–95.
[36] Rabeti MM, Baziar MH. Seismic ground motion amplification pattern induced by a subway tunnel: shaking table testing and numerical simulation. Soil Dyn Earthq Eng 2016;83:81–97.
[37] Yiouta-Mitra P, Kouretzis G, Bouckovalas G, Sofianos A. Effect of underground structures in earthquake resistant design of surface structures. In: Proceedings of the dynamic response and soil properties, new peaks in geotechnics; 2007.
[38] Beskos DE. Boundary element methods in dynamic analysis. Appl Mech Rev 1987;40(1):1–23.
[39] Stamos AA, Beskos DE. Dynamic analysis of large 3-D underground structures by the BEM. Earthq Eng Struct Dyn 1995;24:917–34.
[40] Dominguez J, Meise T. On the use of the BEM for wave propagation in infinite domains. Eng Anal Bound Elem 1991;8(3):132–8.
[41] Crouch SL, Starfield AM. Boundary elements methods in solid mechanics. Department of Civil and Mineral Engineering, University of Minnesota; 1983.
[42] Yang L, Sterling RL. Back analysis of rock tunnel using boundary element method. J Geotech Eng 1989;115(8):1163–9.
[43] Xiao B, Carter JP. Boundary element analysis of anisotropic rock masses. Eng Anal Bound Elem 1993;11:293–303.
[44] Panji M, Asgari Marnani J, Tavousi Tafreshi Sh. Evaluation of effective parameters on the underground tunnel stability using BEM. J Struct Eng Geotech 2011;1(2):29–37.
[45] Wu R, Xu JH, Li C, Wang ZL, Qin S. Stress distribution on mine roof with the boundary element method. Eng Anal Bound Elem 2015;50:39–46.
[46] Panji M, Koohsari H, Adampira M, Alielahi H, Asgari Marnani J. Stability analysis of shallow tunnels subjected to eccentric loads by a boundary element method. JRock Mech Geotech Eng 2016;8:480–8.
[47] Kattis SE, Beskos DE, Cheng HD. 2D dynamic response of unlined and lined tunnels in poroelastic soil to harmonic body waves. Earthq Eng Struct Dyn 2003;32:97–110.
[48] Liu Z, Liu L. An IBEM solution to the scattering of plane SH-waves by a lined tunnel in elastic wedge space. Earthq Sci 2015;28(1):71–86.
[49] Luco JE, DeBarros FCP. Dynamic displacements and stresses in the vicinity of a cylindrical cavity embedded in a half-space. Earthq Eng Struct Dyn 1994;23(3):321–40.
[50] Manolis GD, Beskos DE. Dynamic response of lined tunnels by an isoparametric boundary element method. Comput Methods Appl Mech Eng 1983;36:291–307.
[51] Parvanova SL, Dineva PS, Manolis GD, Wuttke F. Seismic response of lined tunnels in the half-plane with surface topography. Bull Earthq Eng 2014;12(2):981–1005.
[52] Yu MC, Dravinski M. Scattering of a plane harmonic SH wave by a completely embedded corrugated scatterer. Int J Numer Methods Eng 2009;78:196–214.
[53] Panji M, Kamalian M, Asgari Marnani J, Jafari MK. Transient analysis of wave propagations problems by half-plane BEM. Geophys J Int 2013;194(3):1849–65.
[54] Dong CY, Lo SH, Cheung YK. Numerical solution for elastic half-plane inclusion problems by different integral equation approaches. Engineering Anal Bound Elem 2004;28:123–30.
[55] Dong CY, Lo SH. Boundary element analysis of an elastic half-plane containing nanoinhomogeneities. J Comput Mater Sci 2013;73:33–40.
[56] Panji M, Ansari B. Modeling pressure pipe embedded in two-layer soil by a half-plane BEM. Comput Geotech 2017;81:360–7.
[57] Telles JCF, Brebbia CA. Boundary element solution for half-plane problems. Int J Solids Struct 1980;12:1149–58.
[58] Ye GW, Sawada T. Some numerical properties of boundary element analysis using half-plane fundamental solutions in 2-D elastostatics. J Comput Mech 1989;4:161–4.
[59] Ba Z, Yin X. Wave scattering of complex local site in a layered half-space by using a multidomain ibem: incident plane SH waves. Geophys J Int 2016;205:1382–405.
[60] Benites R, Aki K, Yomogida K. Multiple scattering of SH waves in 2-D media with many cavities. Pure Appl Geophys 1992;138(3):353–90.
[61] Alielahi H, Kamalian M, Asgari Marnani J, Jafari MK, Panji M. Applying a time-domain boundary element method for study of seismic ground response in the vicinity of embedded cylindrical cavity. Int J Civil Eng 2013;15:45–54.

[62] Kamalian M, Jafari MK, Sohrabi-Bidar A, Razmkhah A, Gatmiri B. Time-domain two-dimensional site response analysis of non-homogeneous topographic structures by a hybrid FE/BE method. Soil Dyn Earthq Eng 2006;26(8):753–65.
[63] Kamalian M, Gatmiri B, Sohrabi-Bidar A, Khalaj A. Amplification pattern of 2D semi–sine shaped valleys subjected to vertically propagating incident waves. Int J Numer Methods Biomed Eng 2007;23(10):871–87.
[64] Kamalian M, Jafari MK, Sohrabi-Bidar A, Razmkhah A. Seismic response of 2D semi-sines shaped hills to vertically propagating incident waves: amplification patterns and engineering applications. Earthq Spectr 2008;24(2):405–30.
[65] Takemiya H, Fujiwara A. SH-wave scattering and propagation analyses at irregular sites by time domain BEM. Bull Seismol Soc Am 1994;84(5):1443–55.
[66] Belytschko T, Chang HS. Simplified direct time integration boundary element method. J Eng Mech 1988;114(1):117–34.
[67] Hirai H. Analysis of transient response of SH wave scattering in a half-space by the boundary element method. Eng Anal 1988;5(4):189–94.
[68] Panji M, Kamalian M, Asgari Marnani J, Jafari MK. Analyzing seismic convex topographies by a half-plane time-domain BEM. Geophys J Int 2014;197(1):591–607.
[69] Panji M, Kamalian M, Asgari Marnani J, Jafari MK. Antiplane seismic response from semi-sine shaped valley above embedded truncated circular cavity: a time-domain half-plane BEM. Int J Civil Eng 2014;12(2):193–206.
[70] Rice JM, Sadd MH. Propagation and scattering of SH-waves in semi-infinite domains using a time-dependent boundary element method. J Appl Mech 1984;51:641–5.
[71] Eringen AC, Suhubi ES. Elastodynamics. Linear theory, vol. 2. New York: Academic Press; 1975.
[72] Brebbia CA, Dominguez J. Boundary elements an introductory course. Southampton, Boston: Computational Mechanics Publications; 1989.
[73] Dominguez J. Boundary elements in dynamics. Southampton, Boston: Computational Mechanics Publications; 1993.
[74] Ohtsu M, Uesugi S. Analysis of SH wave scattering in a half space and its applications to seismic responses of geological structures. Eng Anal 1985;2(4):198–204.
[75] Reinoso E, Wrobel LC, Power H. Preliminary results of the modeling of the Mexico City valley with a two-dimensional boundary element method for the scattering of SH waves. Soil Dyn Earthq Eng 1993;12(8):457–68.
[76] Ricker N. The form and laws of propagation of seismic wavelets. Geophysics 1953;18(1):10–40.